Computational geometrical and mechanical modeling of woven ceramic composites at the mesoscale

C. Fagiano, Martin Genet, Emmanuel Baranger, Pierre Ladevèze

▶ **To cite this version:**

C. Fagiano, Martin Genet, Emmanuel Baranger, Pierre Ladevèze. Computational geometrical and mechanical modeling of woven ceramic composites at the mesoscale. Composite Structures, 2014, Computational geometrical and mechanical modeling of woven ceramic composites at the mesoscale, 112, pp.146-156. 10.1016/j.compstruct.2014.01.045 . hal-01081418

HAL Id: hal-01081418
https://hal.science/hal-01081418

Submitted on 5 Jan 2017

HAL is a multi-disciplinary open access archive for the deposit and dissemination of scientific research documents, whether they are published or not. The documents may come from teaching and research institutions in France or abroad, or from public or private research centers.

L'archive ouverte pluridisciplinaire **HAL**, est destinée au dépôt et à la diffusion de documents scientifiques de niveau recherche, publiés ou non, émanant des établissements d'enseignement et de recherche français ou étrangers, des laboratoires publics ou privés.

Computational geometrical and mechanical modeling of woven ceramic composites at the mesoscale

C. Fagiano[a,b,*], M. Genet[a,c,d], E. Baranger[a], P. Ladevèze[a]

[a] *LMT-Cachan, ENS-Cachan/CNRS/UPMC/PRES UniverSud Paris, 61 avenue du Président Wilson, 94235 Cachan Cedex, France*
[b] *ONERA, The French Aerospace Lab, F-92322 Chatillon, France.*
[c] *Lawrence Berkeley National Laboratory, One Cyclotron Road MS62-0237, Berkeley, CA-94720, USA*
[d] *Marie-Curie Fellow, University of California at San Francisco, Surgery Department, 505 Parnassus Avenue, San Francisco, CA-94143, USA*

Abstract

Woven composite materials are receiving particular attention in a wide range of specialized aeronautical applications. Reliable numerical prediction tools based on computational modeling are required to quantitatively characterize the role of the microstructure and damage mechanisms at the mesoscale. In this paper, such a computational strategy is illustrated on a generic SiC/SiC plain weave composite with chemical vapor infiltrated matrix. Matrix and tows damage mechanisms are respectively introduced through the use of an anisotropic damage model, and an homogenized model based on a micromechanical model on the fiber scale. The latter is presented in this paper for the first time. Particular attention is paid to the generation of accurate hexahedral meshes, compatible at the tow-tow and tow-matrix interfaces. The mesh quality is analyzed using an error estimator variable based on the strain energy density. Damage predictions obtained using tetrahedral and hexahedral meshes are compared for basic loading cases, illustrating the need for using high quality meshes in the growing community of woven composites computational modeling.

Keywords:
A. Woven ceramic composites, B. mesoscale modeling, C. damage mechanics.

Contents

*Corresponding author, Telephone: +33 1 46 73 45 10
Email address: christian.fagiano@onera.fr (C. Fagiano)

1. Introduction

Composite materials manufactured using textile architectures are receiving a growing interest in the field of advanced structural applications [1]. One of the reasons is related to the fact that the microstructure of fiber preforms can be tailored to satisfy the specific needs for mechanical performance. Other advantages include the ease of handling for automation, the ability to generate complex shapes, and the reduction of delaminations effects thanks to the architecture of the fabrics. However, their mechanical in-plane properties, stiffness as well as strength, are lower than those of UniDirectional (UD) composites. The reason for this drawback is the generally higher fiber undulation, which is due to the textile fiber architecture and to the fabrication process.
Three-dimensional multiscale modeling of the mechanical behaviour of woven composite materials poses a challenge to the development of reliable finite element models able to predict the macroscopic structural response of the mechanical part [2, 3]. At the macroscale level, which is the scale where the whole mechanical part is considered, the fabric is considered as an anisotropic continuous material exhibiting mechanical properties inherited from its meso- and microscale [2, 4]. At the

mesoscopic level, which is the scale of a yarn, the influence of the woven architecture on stress distribution and mechanical properties is considered. Patterns for woven fabrics are defined by the smallest Representative Volume Element (RVE), if it exists, which describes the interlacing of the warp and weft yarns. Fabrics in the dry form are then consolidated with resin via Resin Transfer Molding (RTM), or other processes. Among them, the Chemical Vapor Infiltration (CVI) technique has been studied since the 1960s, and has become quite important commercially for high temperature structural applications [5]. CVI is a slow process, and the obtained composite materials possess some residual porosity and density gradients. Despite these drawbacks, the CVI presents a few advantages. For instance, the low temperature of the process $(900 - 1100°C)$ minimizes fiber damage, and since densification is conducted under essentially no external pressure, fiber arrangement is undisturbed during the process.

Over the years different tools for the geometric modeling of the preform have been combined with finite elements strategies to obtain an appropriate mechanical characterization of the mesoscale. A short overview of the most important contributions in the field of Ceramic Matrix Composites (CMC), elaborated using CVI, is provided herein. TexGen [6] and WiseTex [7, 8] represent the current state-of-the-art in generalized textile modelers. Even though their primary application is in the design and manufacture of fiber-reinforced polymer matrix composites, Nemeth *et al.* [9] compared the two finite element softwares to gain an understanding of their current capability and to assess the potential suitability of these software programs to efficiently generate finite element models of a broad family of woven architectures of CMC. This was done for both idealized weaves (without defects) as well as weaves with various introduced defects. Tetrahedral meshes were used. Both TexGen and WiseTex were useful for generating solid models of the tow geometry. However, it was concluded that none of the programs at their current state of development was able to provide a complete generalized capability to model a CMC. Moreover, there was a lack of consistency in generating well-conditioned finite element meshes of the tows and matrix since interpenetrations between the meshes were generated. A solution often adopted, mainly in the modeling of polymer matrix composites, is to insert a thin matrix layer between all yarns [8, 10, 11, 12], in order to create independent yarn surfaces. These surfaces and the enclosed can be easily meshed using automated meshing tools. However, the thin matrix layers cause either bad quality elements or a very fine mesh size within the layers, and a reduction of the fiber volume fraction that does not correspond

to reality. FE meshes without these artificial matrix layers have been created up to now only for some specific idealized geometries Woo-CS-1997,Kuhn-JCM-1999. A very flexible method to mesh complex geometries and more and more adopted to avoid problems of interpenetration, especially in case of complex preforms, is the voxel method [13]. The main advantage of this method lies in its simplicity since the meshing can be carried out in few operations whatever is the complexity of the geometry. However, it can provide an extremely rough and mesh-dependent representation of local stress and strain fields, especially at material interfaces, leading to bad predictions of damage mechanisms.

A procedure worth being mentioned to develop automated finite element model generation of 2D textile CMC with progressive damage/failure models has been proposed by the Charalambides group at the University of Maryland Baltimore County. Of particular interest is the work of Rao *et al.* [14] who showed results from extensive simulations regarding elastic and matrix cracking properties for plain weave, 4 Harness-Satin (HS), 5HS, and 8HS architectures. A full 3D finite element model of the RVE, roughly represented, was developed containing the individual tows and matrix. The layered matrix model was developed to study the fiber tow architecture and matrix material deposition via the CVI technique. An interesting feature is the modeling of the large scale void (as a central hole) that served as a region of stress concentration such that damage was always predicted to initiate at this location. A localization procedure from the micromechanical models allowed for determination of stresses within individual constituents and respective damage evolution through loss of effective stiffness. It was concluded that a good approximation of the overall response of the material could be obtained, however, their specificities could not be taken into account.

Another contribution is the one of Couégnat *et al.* [15] who proposed a multiscale model for the mechanical characterization of woven ceramic composite materials based on a physical description of the reinforcement, the properties of the constituents and their damage mechanics for the derivation of the effective macroscopic constitutive behavior. At the mesoscale, the geometry of the woven reinforcement is modeled from the yarns interleaving sequence and their geometrical properties. Then, the total bending energy of the textile reinforcement is minimized to calculate its internal geometry in a relaxed state. The matrix is made of a thin layer deposited almost uniformly around the yarns. Boolean operations, performed directly on the FE mesh of the representative

unit cell, are used to generate the final entities, thus avoiding interpenetration between the parts. Afterward, the damage identified experimentally [16] was duplicated in the finite element mesh by creating cracks at the different scales to identify the damage effect tensor. Couégnat's model probably represents the most accurate approach currently available. However, an idealized geometry of the textile is adopted at the mesoscale, *e.g.* uniform cross section of the yarns. Moreover, a layer of matrix is introduced between the yarns in contact to simplify the meshing process and avoid interpenetration. Additional interesting contributions can be found in [9].

The purpose of this paper is to present a strategy for the mesoscale modeling of woven ceramic composites with chemical vapor infiltrated matrix. The attention is restricted to the presentation of the numerical tools developed and the illustration of the procedure. This is done considering an idealized two-dimensional RVE of plain weave textile architecture. The key points of the strategy are overviewed in section 2, in particular the steps concerning the geometrical construction of the RVE, and the subsequent generation of the finite element model. The damage models adopted in the RVE are presented in section 3. Then, numerical results concerning an idealized RVE of a SiC/SiC plain weave textile architecture subjected to uniaxial tension are shown in section 4. Finally, conclusions are drawn and future possible developments are proposed in section 5.

2. Geometrical modeling on the mesoscale

The proposed procedure is composed of two main parts. The first part concerns the geometrical modeling of the RVE of a CVI textile structure, and it was developed within the CATIA V5 framework. The second part concerns the finite element model and analysis of the RVE, and it was performed using Abaqus/Standard 6.10. A summary of the different steps of the procedure is provided below.

2.1. Representative Volume Element (RVE)

The first step concerns the geometrical model of the textile reinforcement. Some of the mesoscopic models proposed in the literature have been reviewed in the previous section. A modeling strategy of particular interest is the one proposed by Hivet and Boisse [17] who developed a consistent 3D geometrical model of 2D fabric elementary cells for appropriate finite element simulations of the forming process prior to matrix impregnation. They performed experimental observations using different optical processes to determine real yarn geometry in different cases of yarn structure

and weaving. One particularity of this model is that it ensures a realistic contact surface between yarns without interpenetration for all types of weaving. Another particularity of the model is that the section shape varies along the trajectory, so that the influence of contact between yarns on their cross section shape can be taken into account. Moreover, their geometrical model is built using the CAD software CATIA V5. The advantage of using CATIA V5 is that any kind of geometry can be generated and improved. Their strategy was adopted in the present procedure to create the fabric elementary cell.

Then, the matrix has to be introduced on the fabric. Two assumptions are made. First, it is assumed that the geometry of the reinforcement does not change after the matrix infiltration. Second, the matrix has a constant thickness all over the reinforcement. **These hypothesis are clear limitations of the current model, but more realistic hypothesis could be made (see *e.g.* [18]) and more involved technics could be used (see *e.g.* [19]) while still using most of the strategy presented here.** Nevertheless, this idealized model for the RVE was conceived to *(i)* validate the procedure and *(ii)* to test the developed numerical tools. Based on these assumptions, the matrix layer is created by just adding an extra thickness to each yarn. Then, a boolean operation is performed, *i.e.* remove operation, between the yarn and the generated entity to remove the first one from the second one. This procedure is carried on for every pair yarn/matrix layer in the model. However, this procedure generates interpenetrations between each matrix layer and the yarns of the RVE lying on the perpendicular direction since the yarns are in contact. Then, boolean operations similar to the previous ones are performed between the interfering parts to avoid interpenetrations, see Figure 1.

2.2. Finite Element Discretization

In the second step of the procedure the parts generated in CATIA V5 are imported in Abaqus Standard 6.10 using the ".CatPart" format. Particular attention is paid to the generation of accurate hexahedral conforming meshes between the interacting parts of the RVE. Compatibility is extremely important because it allows to *(i)* avoid interpenetrations and *(ii)* to impose more accurate interactions between the different parts of the RVE. The idea is to mesh each part independently because it makes easier the generation of appropriate hexahedral meshes. The meshing procedure is carried out as following: first, each part is partitioned using planes conceived with the aim of generating subdomains that are easier to mesh using Abaqus' tools. This planes allow the

user to drive the mesher in such a way that hexahedral meshes can be easily generated. The planes of partition used for the matrix layers and the yarns are shown, respectively, in Figure 2(a) and Figure 2(b). Then, different meshing techniques available in Abaqus can be used on each subdomain. A structured mesh technique or a sweep meshing technique is combined with an advancing front algorithm [20] on each subdomain of the matrix layers, see Figure 2(a). As far as the yarns are concerned, a regular hexahedral mesh is obtained using the sweep meshing technique combined with an advancing front algorithm on each subdomain, see Figure 2(b).

Each mesh is generated in such a way that periodic boundary conditions can be easily applied using multi-point constraint equations. This means that nodes lying on opposite boundary surfaces of the RVE share approximately the same position. Then, a Python script [21] was developed to impose in-plane periodic boundary conditions on the sides of the RVE. This is done using multi-point constraint equations that impose a relative displacement to each pair of nodes sharing the same position on opposite surfaces. All the regions of the RVE in contact have been seeded using the same number of elements and equivalent topology. Another python script was developed to impose perfect compatibility between the nodes in the areas of contact between two parts. The idea is the following: a master and a slave surface are defined for each pair of surfaces in contact. Then, each node lying on the slave surface is moved to satisfy compatibility with the closest node on the master surface. This procedure is applied to all the interacting regions in the RVE. Then, all the discretized matrix layers are merged using available Abaqus tools to have a better representation of the complete matrix of the RVE. Thus, a single instance is generated for the matrix. The yarns are instead kept as independent parts, thus being able to interact with the other parts of the RVE using, for instance, tie constraints or cohesive laws, *i.e.* cohesive elements or cohesive surface interactions [20]. The mesh quality of the RVE is estimated using an error estimator output variable based on the strain energy density. It was selected between the set of error indicator output variables provided by Abaqus/Standard for the whole element [20]. These error indicator output variables are computed through the patch recovery technique of Zienkiewicz and Zhu [22]. The finite element model of the RVE of a plain textile architecture obtained using the proposed procedure is shown in Figure 3.

3. Material modeling on the mesoscale

3.1. Phenomenology and modeling choices

A short description of the damage mechanisms and associated model is reported herein. Damage in 2D woven SiC/SiC consists essentially in the formation of transverse cracks in the matrix and associated interface cracking resulting from deviation of the cracks by the tows and the fibers within the tows (also referred to as debonding). Three main steps can be distinguished during matrix cracking [23, 24]. First, cracks initiate at the inter-yarn macropores where stress concentrations exist. Then, cracks form in the transverse yarns and in the interply matrix. Finally, transverse microcracks initiate in the longitudinal tows. Ultimate failure is dictated by the fibers, which can break statically, or in static or cyclic fatigue, depending on the loading [25, 26]. In the proposed damage model intra-yarn transversal cracking is taken into account by using a damage model similar to the one proposed at LMT-Cachan for laminated composites [27, 28]. Cracks in the longitudinal yarns and associated fiber-matrix debonding are introduced through the use of a model with inelastic deformation, homogenized from the reference fiber scale framework based on shear lag and Weibull theories [29, 30, 31]. This homogenization process links the damage variables used on the mesoscale to micromechanical variables such as crack density and crack openings [32]. Fiber breaking is not considered.

Note that another potentially important aspect of woven CMCs mechanics is the process-induced residual stresses[33, 34]. However, we do not expect them to be significant in SiC/SiC composites as the ones studied in this paper, and did not consider them. That could be improved in the future.

The material model presented in the next sections is the direct mathematical expression of this damage scenario; if other hypothesis would be made, the corresponding part of the model could be modified while keeping the other unchanged. Actually, this is one of the main interest of our multi-scale approach where every mechanism is modeled separately: the strategy can be used along side experimental studies to test out different hypothesis in terms of failure mechanisms. Similarly, if a new material is processed with *e.g.* the same yarns but different matrix, only the corresponding part of the model must be modified, thus reducing the additional development cost.

Even though models based on a single RVE are inherently limited in predicting material failure,

it is reasonable to consider that damage is relatively homogeneous in the structure until initiation of a macroscopic crack **(we are here referring to structure scale homogeneity, not microstructure, or RVE, scale homogeneity)**. This is especially true for CMCs, where there are many toughening mechanisms that prevent damage localization. Similar models have been shown to be extremely reliable to predict material failure [35, 36]. Moreover, it is a mandatory step toward modeling of more localized phenomena based on multi-RVE cells [38].

3.2. Inter-yarn matrix

3.2.1. Elasticity

The matrix is initially isotropic, with Young modulus E^m & Poisson ratio ν^m. Therefore, its elastic behavior is characterized by the following free enthalpy potential:

$$2\rho^m \phi_0^m \left(\underline{\underline{\sigma}}\right) = \underline{\underline{\sigma}} : \underline{\underline{\underline{\underline{E_0^m}}}}^{-1} : \underline{\underline{\sigma}} \tag{1}$$

$$\text{with } \underline{\underline{\underline{\underline{\widehat{E_0^m}}}}}^{-1} = \begin{bmatrix} \frac{1}{E^m} & \frac{-\nu^m}{E^m} & \frac{-\nu^m}{E^m} & 0 & 0 & 0 \\ & \frac{1}{E^m} & \frac{-\nu^m}{E^m} & 0 & 0 & 0 \\ & & \frac{1}{E^m} & 0 & 0 & 0 \\ & & & \frac{1+\nu^m}{E^m} & 0 & 0 \\ & & & & \frac{1+\nu^m}{E^m} & 0 \\ \text{sym} & & & & & \frac{1+\nu^m}{E^m} \end{bmatrix}$$

where $\widehat{\ }$ denotes the classical engineering, or Voigt, notations[39].

3.2.2. Matrix cracking

The damage model used for the matrix is built within Ladevèze's anisotropic and unilateral damage theory, introduced in [40], and revised in [41]. Several models have been derived from this theory, for multiple materials including SiC/SiC composites [42], C/C composites [43], concrete [44], *etc.* The present model is actually a simplified version of the macroscopic damage model already proposed for CMCs [45, 46, 47], including only the matrix damage. It allows to represent anisotropic damage which direction is not known *a priori*. For the sake of simplicity, it is presented here without unilateral effects (see [47, 48] for more details on that aspect).

Thus, the matrix behavior is characterized by the following free enthalpy potential:

$$2\rho^m \phi^m \left(\underline{\underline{\sigma}}, \underline{\underline{\underline{\underline{S^m}}}} \right) = \underline{\underline{\sigma}} : \underline{\underline{\underline{\underline{S^m}}}} : \underline{\underline{\sigma}} \tag{2}$$

where $\underline{\underline{\underline{\underline{S^m}}}}$ is the damage variable–an internal variable in the classical thermodynamic terminology [39, 49]. One initially has $\underline{\underline{\underline{\underline{S^m}}}}\,(t=0) = \underline{\underline{\underline{\underline{E_0^{m-1}}}}}$.

The damage is directly oriented by the local mechanical load, through the use of the following thermodynamic force:

$$\underline{\underline{\underline{\underline{Y^m}}}} = \langle \underline{\underline{\sigma}} \rangle_+ \otimes \langle \underline{\underline{\sigma}} \rangle_+ \tag{3}$$

where $\langle \underline{\underline{\sigma}} \rangle_+$ is the classical part of the stress in the classical sense [39].

A scalar thermodynamic force is now defined:

$$z^m = \sqrt{\mathrm{Tr}\left(\underline{\underline{\underline{\underline{Y^{m2}}}}} \right)} \tag{4}$$

and the damage evolution law finally writes:

$$\underline{\underline{\underline{\underline{\dot{S^m}}}}} = \dot{\alpha^m} \frac{\partial z^m}{\partial \underline{\underline{\underline{\underline{Y^m}}}}} = \frac{\dot{\alpha^m}}{z^m} \underline{\underline{\underline{\underline{Y^m}}}} \tag{5}$$

where α^m is an hardening-like variable, given by:

$$\begin{cases} \alpha^m = \dfrac{1}{E^m} \langle \dfrac{\sqrt{z} - \sigma_0^m}{\sigma_1^m - \sigma_0^m} \rangle_+^2 \\ \dot{\alpha^m} \geq 0 \end{cases} \tag{6}$$

where σ_0^m & σ_1^m are two material parameters, characterizing the initial & saturation stress levels. Details on the numerical implementation of such anisotropic damage models can be found in [48]. **Briefly, the local behavior is solved using a fixed point method, where Aitken's relaxation is used to accelerate convergence. Contrary to most materials models, here the state law is non linear–actually, multi-linear–due to the traction-compression splitting. It is solved using a BFGS quasi-Newton method.**

3.3. Yarns

Because of the frictional sliding at the fiber-matrix interfaces, the internal energy of the loaded yarn is not entirely recoverable through a purely elastic unloading (*i.e.* an hypothetical unloading where all dissipative phenomena such as the sliding of fibers within the matrix would be forbidden) and is actually composed of the recoverable, or free, energy, and the stored energy [32]:

$$\rho^y e^{y,i} = \rho^y \psi^{y,e} + \rho^y \psi^{y,s} \tag{7}$$

As a consequence, the total strain will be composed of a recoverable and a residual part:

$$\underline{\underline{\epsilon^{y,t}}} = \underline{\underline{\epsilon^{y,e}}} + \underline{\underline{\epsilon^{y,r}}} \tag{8}$$

Instead of a formulation based on energy potentials (which are functions of strain and additional internal variables), we prefer a formulation based on enthalpy potentials, *i.e.* written in stress. As a consequence, the recoverable strain, which accounts for elastic deformation of fibers and matrix as well as longitudinal cracking of the matrix, will derive from the free enthalpy potential, while the residual strain, which accounts for fibers sliding within the matrix induced by transversal cracking of the matrix, will derive from the stored enthalpy potential.

We will always refer to the following material orientation: 1 is the fiber direction; 2 is the in-plane transverse direction; and 3 is the out-of-plane transverse direction. The tensors will always be expressed in this particular basis.

3.3.1. Elasticity

The yarn's elastic behavior is characterized by the following free enthalpy potential:

$$2\rho^y \phi_0^{y,e}\left(\underline{\underline{\sigma}}\right) = \underline{\underline{\sigma}} : \underline{\underline{\underline{\underline{E_0^y}}}}^{-1} : \underline{\underline{\sigma}} \tag{9}$$

$$\text{with } \underline{\underline{\underline{\underline{\widehat{E_0^y}}}}}^{-1} = \begin{bmatrix} \frac{1}{E_1^y} & \frac{-\nu_{12}^y}{E_1^y} & \frac{-\nu_{13}^y}{E_1^y} & 0 & 0 & 0 \\ & \frac{1}{E_2^y} & \frac{-\nu_{23}^y}{E_2^y} & 0 & 0 & 0 \\ & & \frac{1}{E_3^y} & 0 & 0 & 0 \\ & & & \frac{1}{2G_{12}^y} & 0 & 0 \\ & & & & \frac{1}{2G_{13}^y} & 0 \\ \text{sym} & & & & & \frac{1}{2G_{23}^y} \end{bmatrix}$$

so that the elastic state law writes:

$$\underline{\underline{\epsilon^{y,e}}}\left(\underline{\underline{\sigma}}\right) = \frac{\partial \rho^y \phi_0^{y,e}}{\partial \underline{\underline{\sigma}}}\left(\underline{\underline{\sigma}}\right) = \underline{\underline{\underline{\underline{E_0^y}}}}^{-1} : \underline{\underline{\sigma}} \tag{10}$$

In a first step, the components of $\underline{\underline{\underline{\underline{E_0^y}}}}$ are computed from the classical rules of mixture:

$$\begin{cases} E_1^y = E^f V^f + E^m V^m \\ \frac{1}{E_2^y} = \frac{1}{E_3^y} = \frac{V^f}{E^f} + \frac{V^m}{E^m} \\ \frac{1}{\nu_{12}^y} = \frac{1}{\nu_{13}^y} = \frac{V^f}{\nu^f} + \frac{V^m}{\nu^m} \\ \nu_{23}^y = \nu^f V^f + \nu^m V^m \\ \frac{1}{G_{12}^y} = \frac{1}{G_{13}^y} = \frac{V^f}{G^f} + \frac{V^m}{G^m} \\ G_{23}^y = G^f V^f + G^m V^m \end{cases} \tag{11}$$

where $V^{f/m}$, $E^{f/m}$, $\nu^{f/m}$ & $G^{f/m}$ are the volume fraction, Young modulus, Poisson coefficient and shear modulus of the undamaged fiber/matrix ($G^{f/m} = E^{f/m}/2\left(1+\nu^{f/m}\right)$).

3.3.2. Matrix longitudinal cracking

In order to represent the damage induced by the longitudinal cracks, we introduce the damage variable d_2^y. Thus, the yarn's damaged behavior is characterized by the following free enthalpy

potential:

$$2\rho^y\phi^{y,e}\left(\underline{\underline{\sigma}},d_2^y\right)=\underline{\underline{\sigma}}:\underline{\underline{\underline{\underline{E}}}}^{y-1}\left(d_2^y\right):\underline{\underline{\sigma}} \tag{12}$$

$$\text{with } \underline{\underline{\underline{\underline{\widehat{E^y}}}}}^{-1}\left(d_2^y\right)=\begin{bmatrix} \frac{1}{E_1^y} & \frac{-\nu_{12}^y}{E_1^y} & \frac{-\nu_{13}^y}{E_1^y} & 0 & 0 & 0 \\ & \frac{1}{E_2^y\left(1-d_2^y\right)} & \frac{-\nu_{23}^y}{E_2^y} & 0 & 0 & 0 \\ & & \frac{1}{E_3^y} & 0 & 0 & 0 \\ & & & \frac{1}{2G_{12}^y\left(1-d_2^y\right)} & 0 & 0 \\ & & & & \frac{1}{2G_{13}^y} & 0 \\ \text{sym} & & & & & \frac{1}{2G_{23}^y\left(1-d_2^y\right)} \end{bmatrix}$$

The state law simply derives from this potential:

$$\underline{\underline{\epsilon}}^{y,e}\left(\underline{\underline{\sigma}},d_2^y\right)=\frac{\partial\rho^y\phi^e}{\partial\underline{\underline{\sigma}}}\left(\underline{\underline{\sigma}},d_2^y\right)=\underline{\underline{\underline{\underline{E}}}}^{y-1}\left(d_2^y\right):\underline{\underline{\sigma}} \tag{13}$$

The evolution of the damage variable d_2^y is driven by the associated thermodynamic force, which also derives from this potential:

$$Y_2^y\left(\underline{\underline{\sigma}},d_2^y\right)=\frac{\partial\rho^y\phi^{y,e}}{\partial d_2^y}\left(\underline{\underline{\sigma}},d_2^y\right)=\frac{\sigma_{22}^2}{2E_2^y\left(1-d_2^y\right)^2}+\frac{\sigma_{12}^2}{4G_{12}^y\left(1-d_2^y\right)^2}+\frac{\sigma_{23}^2}{4G_{23}^y\left(1-d_2^y\right)^2} \tag{14}$$

In a first step, we use the following damage evolution law:

$$\begin{cases} d_2^y\left(Y_2^y\right)=\left(\langle\frac{\sqrt{Y_2^y}-\sqrt{Y_0^y}}{\sqrt{Y_1^y}-\sqrt{Y_0^y}}\rangle_0^1\right)^2 \text{ with } Y_{0/1}^y=\frac{{\sigma_{0/1}^y}^2}{2E_2^y} \\ \dot{d_2^y}\geq 0 \end{cases} \tag{15}$$

where $\langle\rangle_0^1$ denotes the unit part **(*i.e.* the function returning the value itself if it is between 0 and 1, 0 if it is below 0, and 1 if it is above 1)**, and $\sigma_{0/1}$ the initiation/saturation stress. **Note that the model described here follows the hypothesis that yarns longitudinal cracks are oriented by the microstructure. It would be totally straigthforward to make a different hypothesis, and use instead a model similar to the one used for the inter-yarn matrix, *i.e.* where the damage is directed by the load. Actually, in [48], we introduced damage laws where damage evolution is directed by both the**

microstructure and the load, the relative influence of each being a model parameter.

3.3.3. Matrix transverse cracking and associated fiber-matrix debonding

Micro-macro relationships. Instead of expressing the stored enthalpy potential, we prefer deriving the evolution law of the residual strain directly from micromechanical considerations, by following the approach introduced in [32] and extended in [50]. Let us first consider the 1.5D problem of a single fiber within a cracked matrix, where stress fields are described using the classical shear lag framework [30, 31, 51]. The overall response of the system is given in Figure 4, as well as the stress fields within the fiber ans matrix at a given state (A). A reel unloading would bring the system back to the state (C), involving some sliding at the fiber-matrix interface. It is interesting to define a purely elastic unloading, where sliding at the fiber-matrix interface would be forbidden. This would bring the system back to the hypothetical state (A'), where only auto-equilibrated stresses remain. Stress fields in such state are also given Figure 4. We can now clearly define the total strain $\epsilon^{y,t} = \epsilon^{(A)}$, the residual strain $\epsilon^{y,r} = \epsilon^{(A')}$ and the recoverable or purely elastic strain $\epsilon^{y,e} = \epsilon^{(A)} - \epsilon^{(A')}$. In the shear lag approximation, one has:

$$\epsilon^{y,e} = \frac{\sigma}{E_1^y} \tag{16}$$

where $\bar{E} = E^f V^f + E^m V^m$ (see Equation (11)). It is important to notice that this is actually the elastic law of the undamaged material: in such a simple approximation, the cracks induce residual strains but no stiffness reduction. It is not the case for more complex approximations of the stress fields [32].

In order to express the residual strain, let is write it:

$$\epsilon^{y,r} = \frac{u^{y,r}}{l^y} \tag{17}$$

where $u^{y,r}$ is the residual displacement associated to a single crack and l^y the average distance between the cracks within the yarn. The evolution of $u^{y,r}$ depends on loading history. However, if we consider only full loading-unloading cycles, only one additional variable is required to characterize the loading history, namely the maximum applied stress. Thus, in the shear lag approximation,

one has:

$$\begin{cases} \dot{u}^{y,r} = \begin{cases} \dfrac{r^f E^{m2} V^{m2} \sigma \dot{\sigma}}{E_1^{y2} E^f V^{f2} \tau} & \text{on} \quad (OA) \\ -\dfrac{r^f E^{m2} V^{m2} \left(\sigma - \sigma^{(A)}\right) \dot{\sigma}}{2 E_1^{y2} E^f V^{f2} \tau} & \text{on} \quad (AC) \\ \dfrac{r^f E^{m2} V^{m2} \sigma \dot{\sigma}}{2 E_1^{y2} E^f V^{f2} \tau} & \text{on} \quad (CA) \end{cases} \\ u^{y,r} \geq 0 \end{cases} \tag{18}$$

where r^f is the fiber radius. As for the evolution of l^y, using classical Weibull theory, one has:

$$\begin{cases} l^y = L_0 \ln(2) \left(\dfrac{\sigma_0}{\sigma}\right)^m \\ \dot{l^y} \leq 0 \end{cases} \tag{19}$$

where L_0, σ_0 & m are the classical Weibull coefficients.

Back to yarn model. In a first step, we take:

$$\underline{\underline{\epsilon}}^{y,r} = \epsilon^{y,r} \left(\underline{n_1} \, {}^t\underline{n_1}\right) \tag{20}$$

where $\underline{n_1}$ is the fiber direction, and the evolution of $\epsilon^{y,r}$ is given by Equations (17), (18) & (19), in which we take:

$$\sigma = \underline{\underline{\sigma}} : \left(\underline{n_1} \, {}^t\underline{n_1}\right) \tag{21}$$

4. Illustration

The proposed procedure was illustrated on a generic RVE of a plain weave textile architecture subjected to uniaxial tension in the x-direction, see Figure 3. The material properties and the damage thresholds assumed for the yarns and the matrix are based on the study carried on by Lissart and Lamon [52] who investigated the mechanical properties and statistical parameters of SiC/SiC unidirectional composites fabricated using CVI. They are presented Table 1. The unit cell edge length is 5.84 mm, and the cross section width and maximum thickness are, respectively, 2.68 mm and 0.29 mm. The thickness of the sheets of matrix is 20 μm. In-plane periodic boundary conditions were assigned on the sides of the RVE (as explained in section 2) and tie-constraints were imposed between the interacting parts.

Different three-dimensional isoparametric finite elements of Abaqus were compared and evaluated in their suitability to describe the damage initiation and evolution. The attention was restricted to linear finite elements since they are, in general, preferred to quadratic ones when contact interactions are considered [20]. Moreover, they are less computationally expensive. Neither reduced nor selective integration techniques were used. The first mesh was generated using 8-node linear hexahedral elements (C3D8 [20]). The mesh quality of the RVE was evaluated using Abaqus error estimator output variable based on the strain energy density. A converged solution in the stress-strain curve, leading to reasonable error estimations close to the free edges of the RVE, was achieved using a mesh of approximately 90000 elements ($\approx$ 390000 degrees of freedom). It is worth noting that the mesh density assumed here is much finer than the mesh density commonly used in the literature for similar analyses [9]. The stress-strain curve obtained is shown in Figure 5. This curve was calculated as follows: the stresses are calculated as the ratio between the sum of the nodal longitudinal forces and the cross-sectional area of the yarns, whereas the deformations is the ratio between the difference of the imposed displacements on opposite cross sections of the RVE and their distance. The error estimations obtained in the yarns at the beginning of the non-linear mechanical behavior, *i.e.* $\sigma_{11} \approx 60\ MPa$, for compatible hexahedral meshes are shown in Figure 6(a). The most important error is encountered close to the macroporosity where it is on average of 35% over a distance of about 5% the in-plane cell dimension. This is due to the singular stress field at the free edges of the macroporosity. On the other regions the error is always less than 10%. Similar results were obtained using 8-node linear hexahedral incompatible mode elements (C3D8I [20]). However, C3D8I elements are preferred to C3D8 elements in presence of complex states of bending. Compatible tetrahedral meshes were also considered using 4-node linear tetrahedral elements (C3D4 [20]). The final mesh had approximately the same number of nodes generated using hexahedral compatible meshes. The stress-strain curve obtained overlaps the one obtained using C3D8 elements, see Figure 5. However, the estimates of the solution error in the strain energy density are much bigger compared to the ones obtained using C3D8 elements, see Figure 6(b). In most of the regions the error is between 40% and 80%. The error close to the macroporosity is on average of 110% over a distance of about 5% the in-plane cell dimension.

Both hexahedral and tetrahedral meshes provide a sequence of damage mechanisms similar to the expected ones for woven CMC subjected to uniaxial tension [24]. First, cracks initiate at the inter-

yarn macropore where stress concentrations exist. Inter-yarn matrix damage distribution on the RVE obtained at the end of the analysis using hexahedral compatible meshes is shown in Figure 7. As expected, matrix damage is mainly concentrated close to the macropore. Then, cracks form in the transverse yarns. Intra-yarn transversal cracking distribution on the RVE obtained at the end of the analysis using hexahedral compatible meshes is shown in Figure 8. As a consequence of the matrix damage distribution, intra-yarn damage is also mainly concentrated close to the macropore. Finally, transverse microcracks initiate in the longitudinal tows. Distributions concerning the intra-yarn longitudinal cracking on the RVE obtained at the end of the analysis using hexahedral and tetrahedral meshes are shown, respectively, in Figure 9(a) and 9(b). Intra-yarn longitudinal cracking is lower than intra-yarn transversal cracking close to the macropore confirming the expected sequence of damage mechanisms. It is important to remark that similar damage distributions are obtained using hexahedral and tetrahedral meshes, even though the error estimations concerning the strain energy density are quite different. This is because only the in-plane stress fields are taken into account in the adopted damage models, and not the transverse ones which have a major impact on the solution errors of the strain energy density distributions. This is due to the difficulties commonly encountered in the modeling of the transverse stress fields close to free edges. It can be stated that important errors on the evaluation of the strain energy density may have major effects in the prediction of the damage mechanisms if cohesive interactions between the parts are introduced a cause of the direct influence of the transverse stress fields.

It is important to recall that these preliminary results are obtained using *(i)* an idealized, one single layer geometry of the RVE and *(ii)* tie-constraints between the parts in contact instead of more realistic interactions, *e.g.* cohesive zones. Another aspect that is worth to clarify is that the values of the damage variables obtained using hexahedral meshes can provide negative values once extrapolated from the integration points to the nodes. This is because the extrapolation is done using the shape functions of the isoparametric linear hexahedron. In fact, these functions vary linearly on quadrilateral coordinate lines, but are not linear polynomials as in the case of tetrahedron, see Figure 9. However, the damage values provided at the integration points are correct, then the problem concerns only the visualization module of Abaqus/CAE .

Matrix				Fibers		
Elasticity		Damage		Geometry	Elasticity	
E^m (GPa)	ν^m ()	σ_0^m (MPa)	σ_1^m (MPa)	r^f (μm)	E^f (GPa)	ν^f ()
400	0.2	25	100	7	200	0.2

Fiber-Matrix interface	Yarns			
Damage	Geometry		Damage	
τ (GPa)	V^f (%)	V^m (%)	σ_0^y (MPa)	σ_1^y (MPa)
100	30	60	50	200

Table 1: Numerical values for the mechanical model's parameters, corresponding to a generic SiC/SiC composite [24, 52]

5. Conclusion

The strategy presented in this paper is conceived with the aim of avoiding some of the numerical problems commonly encountered using most of the methodologies proposed in the literature for the mesoscale modeling of ceramic woven composites. For instance, yarn-yarn and yarn-matrix interactions are numerically corrects by imposing conforming meshes between the interacting parts of the RVE. Moreover, conforming meshes are generated using both tetrahedral and hexahedral elements. As a consequence, there is no need to introduce an additional layer of matrix between the yarns in contact to generate a mesh without interpenetration, as commonly done in the literature. Thus, the procedure generates a computational geometrical model of the RVE suitable for future inter-yarn damage analyses, e.g. delamination, requiring an appropriate evaluation of the energy dissipation at the contact interfaces. By using classical error estimators, we found that tetrahedral elements could induce up to 110% error close to stress concentration areas, while with hexahedral elements the error was bounded to 35%. This is of particular interest since most of the meshing strategies proposed in the literature are based on tetrahedrons. In terms of mechanical modeling, similar distributions of the damage variables were obtained, even though the error estimations concerning the strain energy density were quite different. This is because only the in-plane stress field is taken into account in the adopted damage models, and not the transverse one which has a major impact on the solution errors of the strain energy density distributions. This is due to the difficulties commonly encountered in the modeling of the transverse stress field close to free edges. This also means that important errors on the evaluation of the strain energy density would have major effects in the prediction of the damage mechanisms if cohesive interactions between the parts are introduced. This is a cause of the direct influence of the transverse stress field.

We can conclude that the model presented here, though in early stage of development, is already able to reproduce most of the main features of CMCs behavior law. However, an appropriate validation with experimental data available in the literature could not be done at this state of the work. This is because an idealized RVE of a plain weave textile architecture was adopted to facilitate the presentation of the method and to provide guidelines for further developments. Future research will concern the geometrical and mechanical characterization of real RVEs of woven ceramic composites having different preforms, *e.g.* satin and interlock, and conceived for industrial applications. RVEs of multilayer woven architectures will be also developed, and the effects of nesting in the prediction and propagation of damage will be analyzed. Great attention will be paid to the development and identification of appropriate cohesive interactions between the parts.

Acknowledgments

The authors want to thank the financial support of the project ARCOCE and COMPTINN which have partially founded this study. SAFRAN Herakles is also acknowledged for its constant support.

References

[1] D. Coupé, Composite reinforcements for optimum performance, Edited by Boisse P., Woodhead Publishing, 2011.

[2] S. Flores, A. G. Evans, F. W. Zok, M. Genet, B. N. Cox, D. B. Marshall, O. Sudre, Q. D. Yang, Treating matrix nonlinearity in the binary model formulation for 3D ceramic composite structures, Composites Part A: Applied Science and Manufacturing 41 (2) (2010) 222–229. doi:10.1016/j.compositesa.2009.10.020.

[3] M. Ansar, W. Xinwei, Z. Chouwei, Modeling strategies of 3D woven composites: A review, Composite Structure, 93(8) (2011) 1947–1963.

[4] L. Marcin, J.-F. Maire, N. Carrere, E. Martin, Development of a Macroscopic Damage Model for Woven Ceramic Matrix Composites, International Journal of Damage Mechanics 20 (6) (2010) 939–957. doi:10.1177/1056789510385259.

[5] F. Christin, Design, fabrication, and application of thermostructural composites like C/C, C/SiC, and SiC/SiC composites, Advanced Engineering Materials 4 (2002) 895–912.

[6] M. Sherburn, Geometric and mechanical modelling of textiles, Ph.D. thesis, The University of Nottingham (2007).

[7] S. Lomov, A. Gusakov, G. Huysmans, A. Prodromou, I. Verpoest, Textile geometry preprocessor for meso-mechanical models of woven composites, Composites Science and Technology 60 (11) (2000) 2083–2095.

[8] S. Lomov, D. Ivanov, I. Verpoest, M. Zako, T. Kurashiki, H. Nakai, Meso-FE modelling of textile composites: Road map, data flow and algorithms, Composites Science and Technology 67 (9) (2007) 1870–1891.

[9] N. Nemeth, S. Mital, J. Lang, Evaluation of solid modeling software for finite element analysis of woven ceramic matrix composites, Tech. rep., NASA/TM-2010-216250 (2010).

[10] N. De Carvalho, S. Pinho, P. Robinson, Numerical modelling of woven composites: Biaxial loading, Composites Part A: Applied Science and Manufacturing 43 (8) (2012) 1326–1337.

[11] A. Melro, P. Camanho, F. Andrade Pires, S. Pinho, Numerical simulation of the non-linear deformation of 5-harness satin weaves, Computational Materials Science 61 (2012) 116–126.

[12] S. Lomov, P. Boisse, E. Deluycker, F. Morestin, K. Vanclooster, D. Vandepitte, al., Full-field strain measurements in textile deformability studies, Composites Part A: Applied Science and Manufacturing 39 (8) (2008) 1232–1244.

[13] J. Schneider, G. Hello, Z. Aboura, M. Benzeggagh, D. Marsal, A meso-FE voxel model of an interlock woven composite, in: Proceeding of the International Conference in Composite Materials 17th (ICCM17), Edinburgh, Scotland, 2009.

[14] M. Rao, M. Pantiuk, P. Charalambides, Modeling the geometry of satin weave fabric composites, Journal of composite materials 43 (1) (2009) 19–56.

[15] G. Couégnat, E. Martin, J. Lamon, N. Carrère, Multiscale modeling of the mechanical behaviour of woven composite materials, in: Proceeding of the International Conference in Composite Materials 17th (ICCM17), Edinburgh, Scotland, 2009.

[16] P. Pineau, G. Couégnat, J. Lamon, Virtual testing applied to transverse multiple cracking of tows in woven ceramic composites, Mechanics Research Communications 38 (8) (2011) 579–585.

[17] G. Hivet, P. Boisse, Consistent 3d geometrical model of fabric elementary cell. application to a meshing preprocessor for 3d finite element analysis, Finite Elements in Analysis and Design 42 (2005) 25–49.

[18] A. Vanaerschot, B. N. Cox, S. V. Lomov, D. Vandepitte, Stochastic multi-scale modelling of textile composites based on internal geometry variability, Computers & Structures, 122 (2013) 55–64.

[19] B. Tranquart, P. Ladevze, E. Baranger, A. Mouret, A computational approach for handling complex composite microstructures, Composite Structures, 94(6), 2097–2109.

[20] ABAQUS, Inc., ABAQUS Version 6.10 User's Manual, Pawtucket, RI, USA.

[21] ABAQUS, Inc., ABAQUS Version 6.10 Scripting User's Manual, Pawtucket, RI, USA.

[22] O. C. Zienkiewicz, J. Z. Zhu, The superconvergent patch recovery and a posteriori error estimates. part 1: The recovery technique, International Journal for Numerical Methods in Engineering 33 (7) (1992) 1331–1364.

[23] P. Ladevèze, A. Gasser, O. Allix, Damage mechanisms modelling for ceramic composites, Journal of Engineering Materials and Technology 116 (1994) 331–336.

[24] J. Lamon, A micromechanics-based approach to the mechanical behavior of brittle-matrix composites, Composites Science and Technology 61 (2001) 2259–2272.

[25] W. Gauthier, J. Lamon, Delayed Failure of Hi-Nicalon and Hi-Nicalon S Multifilament Tows and Single Filaments at Intermediate Temperatures (500C-800C), Journal of the American Ceramic Society 92 (3) (2009) 702–709. doi:10.1111/j.1551-2916.2009.02924.x.

[26] P. Ladevèze, M. Genet, A new approach to the subcritical cracking of ceramic fibers, Composites Science and

Technology 70 (11) (2010) 1575–1583. doi:10.1016/j.compscitech.2010.04.013.

[27] P. Ladevèze, E. Le Dantec, Damage modelling of the elementary ply for laminated composites, Composites Science and Technology 43 (3) (1992) 257–267. doi:10.1016/0266-3538(92)90097-M.

[28] O. Allix, P. Ladevèze, Interlaminar interface modeling for the prediction of delamination, Composite Structures 22 (4) (1992) 235–242.

[29] W. Weibull, A statistical theory of the strength of materials, Royal Swedish Institute for Engineering Research 151.

[30] J. Aveston, G. A. Cooper, A. Kelly, Single and multiple fracture, in: Proceedings of the Conference of the National Physical Laboratory on the Properties of Fiber Composites, Vol. 4, 1971, pp. 15–26.

[31] W. A. Curtin, Theory of mechanical properties of ceramic matrix composites, Journal of the American Ceramic Society 74 (11) (1991) 2837–2845.

[32] F. Hild, A. Burr, F. A. Leckie, Matrix cracking and debonding of ceramic-matrix composites, International Journal of Solids and Structures 33 (8) (1996) 1209–1220.

[33] J. W. Kim, D. G. Lee, Measurement of residual stresses in thick composite cylinders by the radial-cut-cylinder-bending method, Composite Structures 77(4) (2007) 444456.

[34] Y. Xua, T. You, Minimizing thermal residual stresses in ceramic matrix composites by using Iterative MapReduce guided particle swarm optimization algorithm, Composite Structures 99 (2013) 388396.

[35] M. R. Begley, N. R. Philips, B. G. Compton, D. V. Wilbrink, R. O. Ritchie, M. Utz, Micromechanical models to guide the development of synthetic "brick and mortar" composites, Journal of the Mechanics and Physics of Solids 60 (8) (2012) 1545–1560. doi:10.1016/j.jmps.2012.03.002.

[36] M. Genet, M. Houmard, S. Eslava, E. Saiz, A. P. Tomsia, A two-scale Weibull approach to the failure of porous ceramic structures made by robocasting: Possibilities and limits, Journal of the European Ceramic Society 33 (4) (2013) 679–688. doi:10.1016/j.jeurceramsoc.2012.11.001.

[37] M. Genet, A. P. Tomsia, R. O. Ritchie, An homogenized damage model for ceramic structures made by freeze-casting, in: 10th World Congress on Computational Mechanics, 2012.

[38] M. Genet, G. Cougnat, A. P. Tomsia, R. O. Ritchie, Scaling strength distributions in quasi-brittle materials from micro to macro scales: A computational approach to modeling Nature-inspired structural ceramics (Submitted for publication). Mechanics, 2012.

[39] J. Lemaître, J.-L. Chaboche, R. Desmorat, A. Benallal, Solid Materials Mechanics, Third Edition (In French), Dunod, 2009.

[40] P. Ladevèze, On an anisotropic damage Theory (in French), Internal report 34, LMT-Cachan (Mar. 1983).

[41] P. Ladevèze, An anisotropic damage theory with unilateral effects: applications to laminate and three- and four-dimensional composites, in: O. Allix, F. Hild (Eds.), Continuum Damage Mechanics of Materials and Structures, Elsevier, 2002, pp. 205–233.

[42] A. Gasser, P. Ladevèze, M. Poss, Damage Mechanismes of Woven SiC/SiC Composite: Modeling and Identification, Composites Science and Technology 56 (7) (1996) 779–784.

[43] X. Aubard, C. Cluzel, L. Guitard, P. Ladevèze, Modelling of the mechanical behavior of 4D carbon/carbon composite materials, Composites Science and Technology 58 (1998) 701–708.

[44] R. Desmorat, F. Gatuingt, F. Ragueneau, Nonlocal anisotropic damage model and related computational aspects for quasi-brittle materials, Engineering Fracture Mechanics 74 (10) (2007) 1539–1560. doi:10.1016/j.engfracmech.2006.09.012.

[45] P. Ladevèze, S. Letombe, C. Cluzel, A CMC damage model based on micro and macromechanics for high-temperature and complex loading, in: Proceedings of the 4th International Conference on High Temperature Ceramic Matrix Composites (HTCMC4), 2001.

[46] C. Cluzel, E. Baranger, P. Ladevèze, A. Mouret, Mechanical behaviour and lifetime modelling of self-healing ceramic-matrix composites subjected to thermomechanical loading in air, Composites Part A: Applied Science and Manufacturing 40 (8) (2009) 976–984. doi:10.1016/j.compositesa.2008.10.020.

[47] M. Genet, L. Marcin, E. Baranger, C. Cluzel, P. Ladevèze, A. Mouret, Computational prediction of the lifetime of self-healing CMC structures, Composites Part A: Applied Science and Manufacturing 43 (2) (2012) 294–303. doi:10.1016/j.compositesa.2011.11.004.

[48] M. Genet, L. Marcin, P. Ladevèze, On structural computations until fracture based on an anisotropic and unilateral damage theory, International Journal of Damage Mechanics (Accepted).

[49] J. Lemaître, A Course on Damage Mechanics, Second Edition, Springer-Verlag, 1996.

[50] M. Genet, Toward a virtual material for ceramic composites (in French), Phd thesis, ENS-Cachan (2010).

[51] W. A. Curtin, Multiple matrix cracking in brittle matrix composites, Acta Metallurgica et Materialia 41 (5) (1993) 1369–1377.

[52] N. Lissart, J. Lamon, Damage and failure in ceramic matrix minicomposites: Experimental study and model, Acta Materialia, 4(3) (1997) 1025–1044.

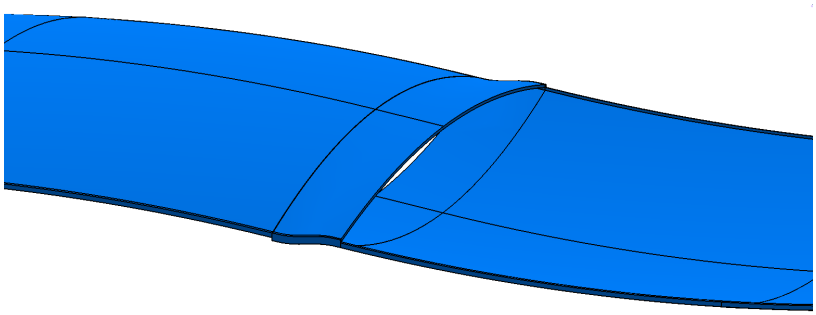

Figure 1: Layer of matrix after the use of boolean operators

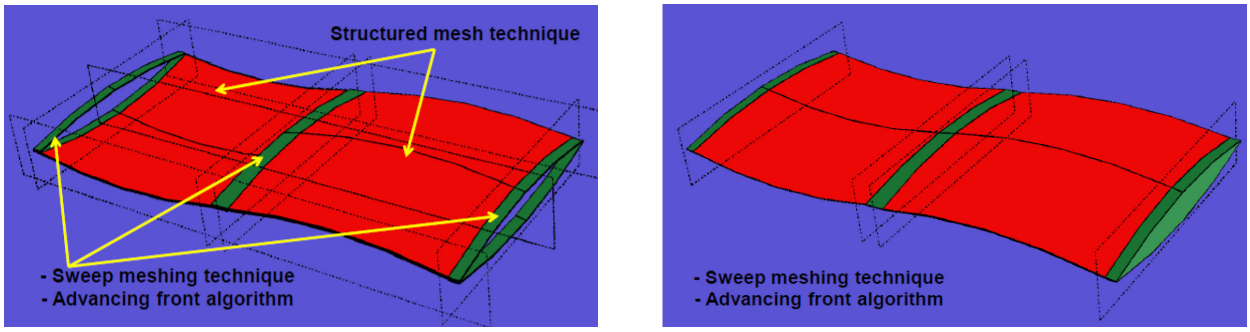

(a) Partition planes on the matrix layers

(b) Partition planes on the yarns

Figure 2: Partition planes created on the different parts of the RVE for plain textile architecture

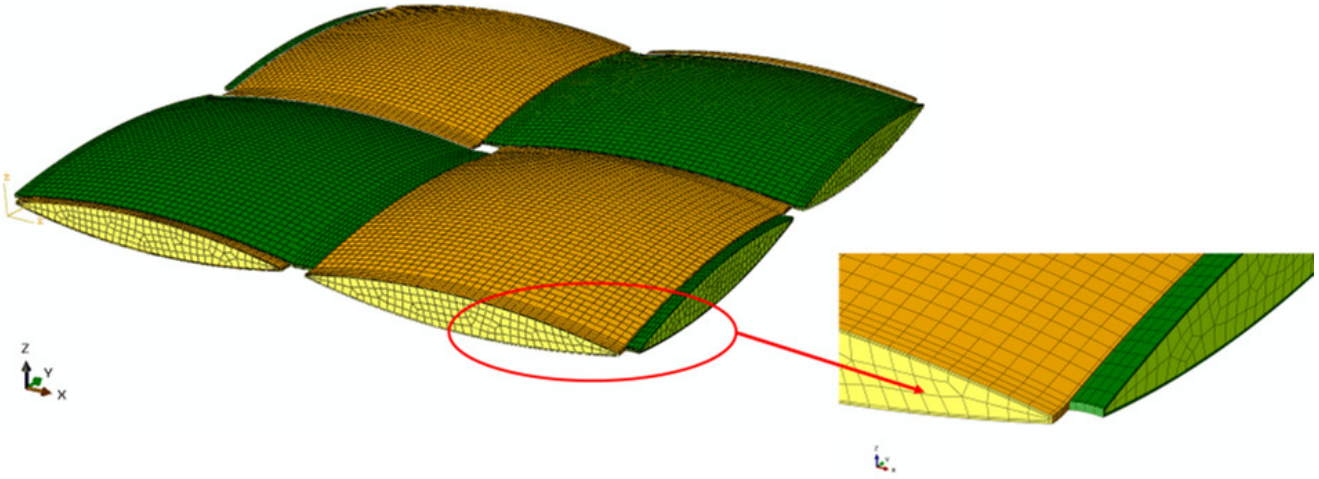

Figure 3: Finite element model of the RVE of a plain textile architecture elaborated using CVI

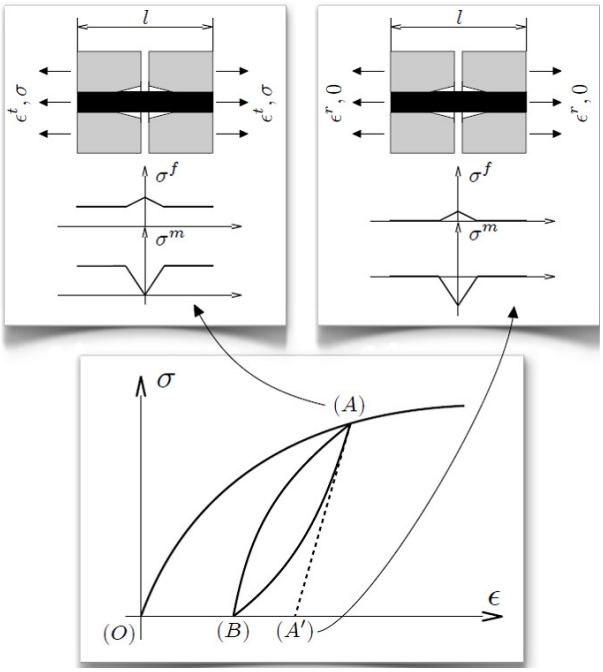

Figure 4: Decomposition of the internal energy into recoverable and stored parts, leading to the decomposition of the total strain into recoverable and residual parts

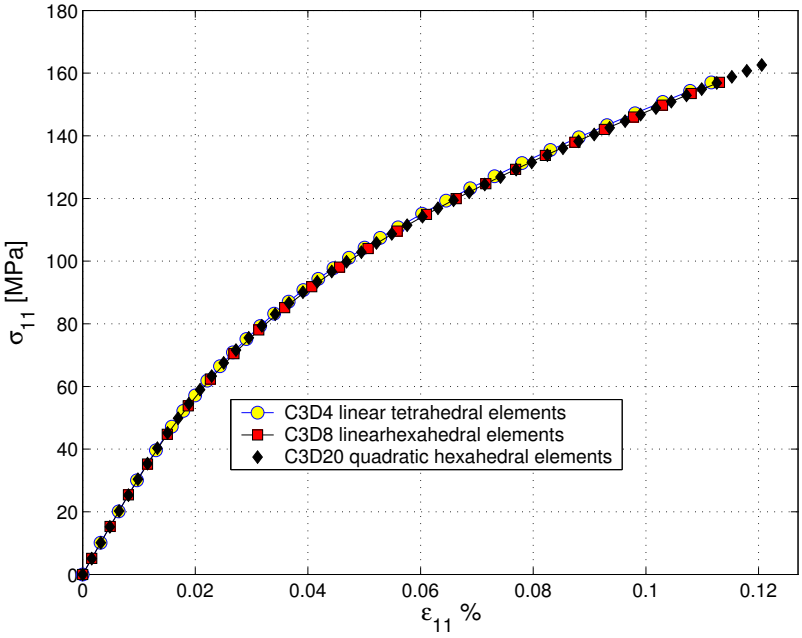

Figure 5: Stress-strain curve obtained using different finite elements

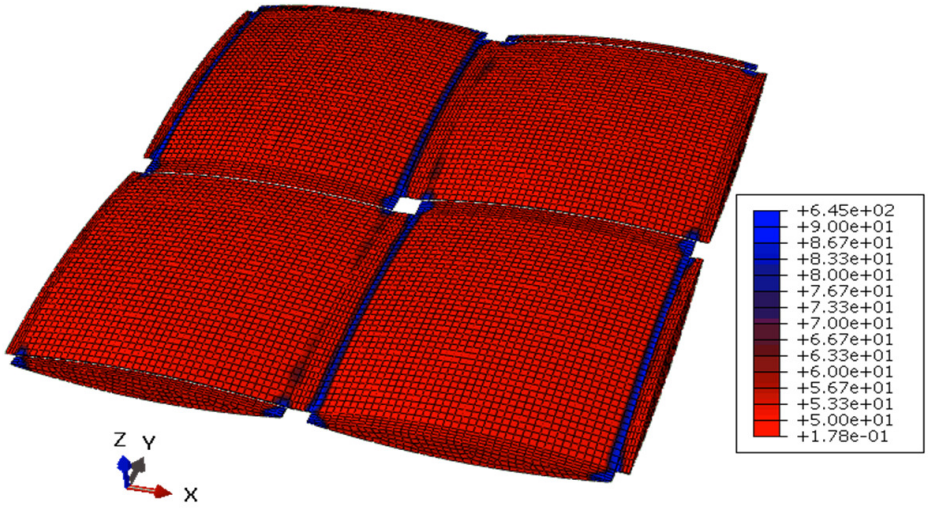

(a) Hexahedral compatible meshes

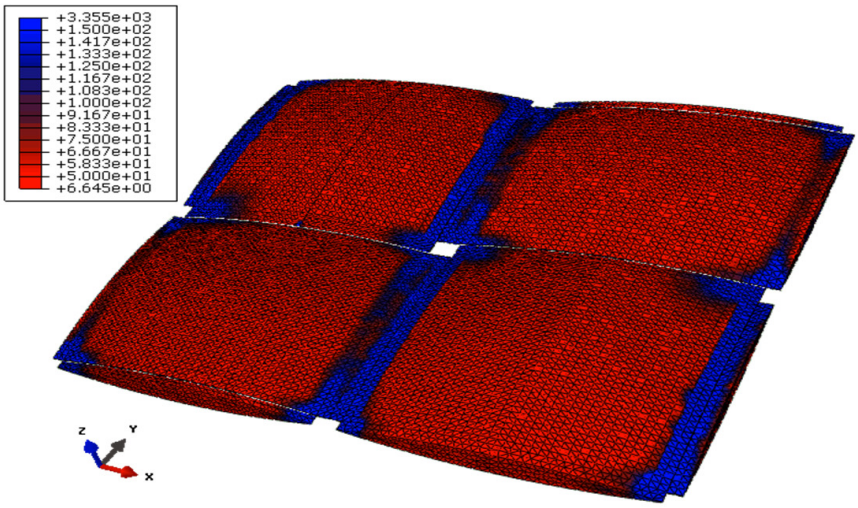

(b) Tetrahedral compatible meshes

Figure 6: Strain energy density error distribution on the yarns of the RVE

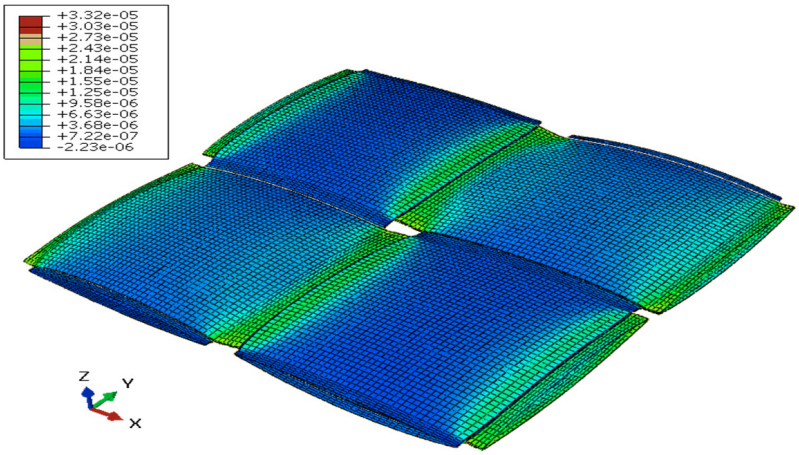

Figure 7: Inter-yarn matrix damage distribution on the RVE obtained using hexahedral compatible meshes (α^m, see Section 3) (note that α^m must be multiplied by E^m, here 400 GPa, or 4 10^5 MPa, to be in the range $[0;1]$, hence the magnitude of 10^{-5})

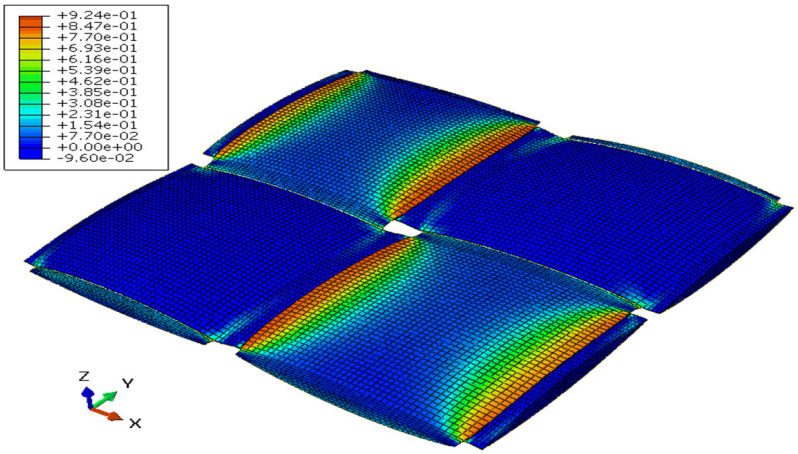

Figure 8: Intra-yarn transversal cracking distribution on the RVE obtained using hexahedral compatible meshes (d_2^y, see Section 3)

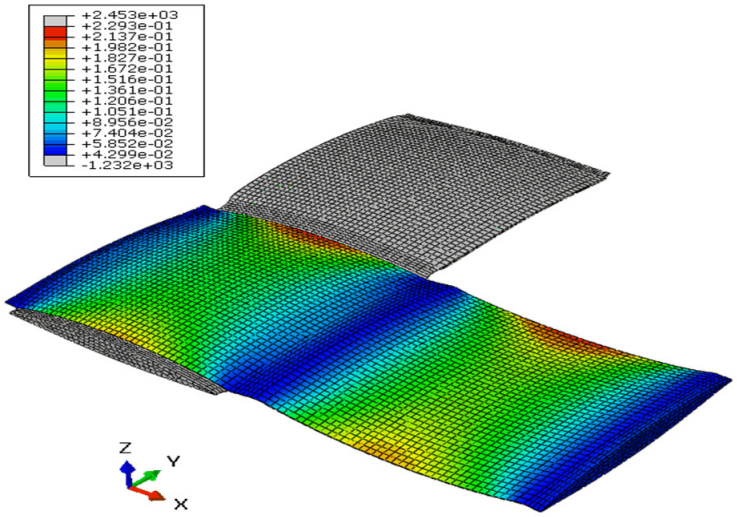

(a) Hexahedral compatible meshes

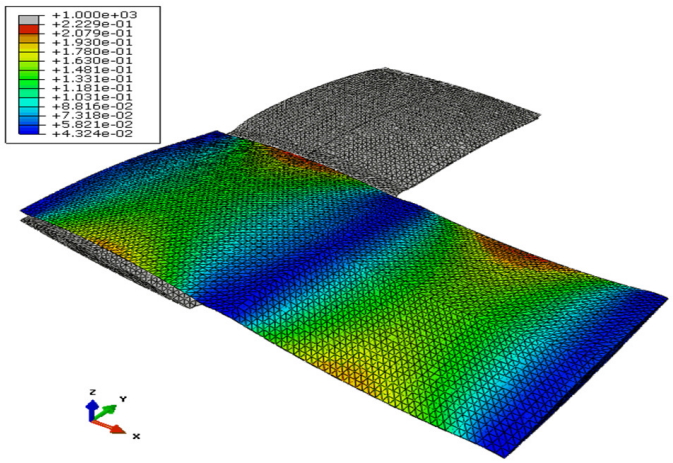

(b) Tetrahedral compatible meshes

Figure 9: Intra-yarn longitudinal cracking distribution on the RVE (l^y, see Section 3, in mm)